Effects of externally applied stress on the properties of quantum dot nanostructures

H. T. Johnson and R. Bose
Department of Mechanical and Industrial Engineering, University of Illinois at Urbana-Champaign, Urbana, Illinois 61801

B. B. Goldberg
Department of Physics, Boston University, Boston, Massachusetts, 02215

H. D. Robinson
Department of Electrical Engineering, University of California at Los Angeles, Los Angeles, California, 90095

Abstract

An array of semiconductor quantum dots is studied computationally using an approach that couples linear elasticity to electronic and optical properties. The effect of strain on the photoemission behavior of the quantum dot array is of particular interest. With a realistic quantum dot array morphology as input, finite element analysis is first used to compute electron energy levels in the domain. From these energy levels, optical conductivity is computed for the system, which is directly comparable with experimental optical absorption and emission spectra. Then, to simulate the effect of microscope tip-sample interaction, the strain field associated with a rigid cylindrical indenter is superimposed on the sample and the calculation is performed again. The computed optical spectrum shows a distinct blue-shift as a result of the indentation strain field. This observation is qualitatively and quantitatively in agreement with near field scanning optical microscopy (NSOM) experiments on the same material system. The result shows that in nanoscale semiconductor devices, mechanical and electronic properties are coupled over the same length scales and can be treated together in a coupled continuum finite element formulation.

1. INTRODUCTION

Semiconductor quantum dots are nanometer scale clusters of material with unique electronic and optical properties derived from their quantum mechanical behavior. Quantum dot arrays have received tremendous interest recently due to a number of promising applications including photodetectors and photoemitters, the latter being precursors to high quality, low threshold-current lasers. (Bimberg, *et al.* 1999) Due to fabrication and characterization processes, however, these structures are often highly strained, with large variations in strain occurring over lengths as small as several nanometers. At these length scales, it is possible to view both electronic and mechanical behavior from a continuum perspective. Furthermore, both electronic and mechanical behavior can be modeled using linear finite element analysis over the same computational domain, and discretized using the same mesh. In this paper, the particular case of optical properties of a self-assembled quantum dot array with a nonuniform applied stress is considered.

While the mechanics of strain induced self-assembly of a semiconductor quantum dot array is a complex and rich problem, stress analysis of the system alone is not useful in comparing to experimental characterization data. For a wide class of applications, including those considered here, the results of interest are based on optical absorption and emission spectra, or the intensity of absorbed or emitted light as a function of the frequency of that light.

The emission and absorption of light in a semiconductor quantum structure is mediated by transitions between available electron energy levels in the material. The strongest observed transitions in such systems are of the interband type, where photons of a particular energy (related to frequency through $E=\hbar\nu$) cause electron transitions between the valence band and the conduction band. Thus, the bandgap energy of the semiconductor material partially determines the frequency of light that would be absorbed (as a valence band electron is promoted to the conduction band) or emitted (as a conduction band electron decays to the valence band).

Mechanical behavior plays a role in the system because the available electron energy levels, which depend on the underlying electronic structure of the single crystalline material, are sensitive to strain. Strain in the quantum dot array systems is due to either intrinsic effects such as lattice mismatch, which is generally on the order of several percent at most, or external effects such as interactions with nanomechanical probes. While intrinsic strain is small and elastic by design, externally applied strain may be much larger and lead to dislocation nucleation. However, dislocations have overwhelming electrical effects in the systems and must be avoided for device purposes.

1.1 On the choice of modeling methods

To simulate optical properties of semiconductors, it is necessary to compute electron energy levels in the material. However, there are no materials modeling approaches based on fully empirical atomistic methods yielding this information. To perform an atomistic analysis, a method with some quantum mechanical basis would be necessary. But any such methods, from density functional theory to semi-empirical tight-binding, would be impossibly computationally intensive for the systems of interest. Due to the extended or delocalized nature of some important electronic effects in these systems, it is necessary to consider arrays of at least tens of quantum dots, which may include tens of millions of atoms. With these restrictions, the only alternative is a continuum method. While it is significantly less accurate than quantum mechanical atomistic methods, the obvious continuum choice is the well-known k·p Hamiltonian method, which is used to compute energy levels of single, ballistic charge carriers within the effective mass approximation, which averages over the underlying crystalline potential. Importantly, the k·p Hamiltonian method includes a means of incorporating strain effects, which are of direct interest here.

Atomistic methods are also available to compute mechanical behavior of semiconductor quantum dot systems. But within the several nanometer length scale range and for small elastic strains, continuum elasticity is convenient and accurate. While the structures of interest are extremely small, continuum elasticity is known to be reliable down to several atomic spacings for many well-characterized problems, such as in dislocation mechanics.

1.2 Overview and layout of the paper

In this paper, a fully coupled continuum approach is described for the problem of strain effects on optical properties of quantum dot arrays. Starting with a realistic computational mesh for the system of interest, an array of approximately 30 quantum dots embedded between a substrate and a capping layer, finite element analysis is used to compute conduction electron and valence electron (or hole) energy levels. From these energy levels, the optical conductivity of the system, which depends on photon mediated energy level transitions, is computed directly. Elastic strain is incorporate directly in the calculation of the energy levels, so both intrinsic and extrinsic sources of strain are considered. This method is explained in the next section. By considering the strain induced by tip-sample interactions, the optical conductivity of the system is then compared directly to near-field scanning optical microscopy (NSOM) experiments. The results of this comparison, and the implications of the results, are discussed in the final section.

2. MODEL AND FORMULATION

In the following finite element analysis of electronic and optical properties of a strained quantum dot array, a single three-dimensional finite element mesh is used throughout. Part of the domain under consideration is shown in Figure 1. The system consists of a single crystal $Al_{0.35}Ga_{0.65}As$ substrate beneath a few nm thick $In_{0.55}Al_{0.45}As$ "wetting layer", on top of which are approximately 30 $In_{0.55}Al_{0.45}As$ spherical cap shaped quantum dots of 15-20nm in diameter. These features are shown in Figure 1. An $Al_{0.35}Ga_{0.65}As$ capping layer of several nm thickness (not shown in Figure 1) buries the quantum dots. The entire domain is then approximately 220nm by 220nm square in the plane normal to the growth direction, and roughly 30nm thick in the growth direction.

2.1 Input: from morphology studies

The quantum dot array shown in Figure 1 is closely comparable to sections of experimentally grown samples in which the quantum dot array is found to self-assemble, described for example by Leon *et al.* (1995). Real samples would be much larger in lateral dimension, but for the purposes of both the experimental and computational work in question, only a small representative section of an array is of interest. The mesh shown in Figure 1, in fact, is taken from results of a continuum finite element simulation of that process, reported by Zhang and Bower (1999). Important features of the system include the average dot size (approximately 18nm diameter), the irregularity of the dot size and shape, the wetting layer thickness (approximately 2nm), the partial but incomplete spatial ordering of the dots, and the areal dot density. Furthermore, the full three dimensional non-uniform strain field, induced by the lattice mismatch between $Al_{0.35}Ga_{0.65}As$ and $In_{0.55}Al_{0.45}As$, is particularly important. Nearly all of these features are computed accurately by Zhang and Bower (1999) and are thus suitable input for the calculation of strain effects on electronic and optical properties.

2.2 Electron energy levels

In the continuum view of energy band structure for a semiconductor material, electron energy levels can be computed by considering the behavior of a single, extra ballistic charge carrier added to a region of material. Use of the $k \cdot p$ Hamiltonian approach to solve this problem for strained materials is described in detail elsewhere, (Johnson and Freund, 2001) but is briefly reviewed here.

A single charge carrier in an energy subband, typically the conduction band, heavy hole valence subband, or light hole valence subband in a III-V compound such as InAlAs or AlGaAs, is modeled using the steady state Schrödinger equation in the effective mass approximation. Thus, the unknown wave functions Ψ and energies E can be found from the equation:

$$(1) \qquad \frac{-\hbar^2}{2m_*}\nabla^2\Psi^\beta(\vec{r}) + V^{\alpha\beta}(\vec{r})\Psi^\beta(\vec{r}) = E\Psi^\alpha(\vec{r})$$

where m_* is the effective mass of the charge carrier. In the more accurate k·p formulation, which includes perturbation of the wave vector k by the momentum p of the particle, the energy subbands are coupled. The resulting governing equation is given by:

$$(2a) \qquad H^{\alpha\beta}_{k\cdot p}(\vec{r})\Psi^\beta(\vec{r}) + V^{\alpha\beta}(\vec{r})\Psi^\beta(\vec{r}) = E\Psi^\alpha(\vec{r})$$

where

$$(2b) \qquad H^{\alpha\beta}_{k\cdot p}(\vec{r}) = \frac{-\hbar^2}{2m_0}\nabla_i L^{\alpha\beta}_{ij}(\vec{r})\nabla_j$$

where the Hamiltonian contains the Luttinger-Kohn tensor L, which modifies and couples the effective masses in the multiple subband basis. Here m_0 is the reference effective mass of an electron in free space.

Strain affects the potential energy V, which describes the local environment that the charge carrier experiences. For the purposes of the analysis here, V is considered to contain only (i) the effects of the local band gap energy offset relative to some reference point, and (ii) the strain contribution, so that it can be written as:

$$(3) \qquad V^{\alpha\beta} = V^{\alpha\beta}_{bg} + D^{\alpha\beta}_{ij}\varepsilon_{ij}$$

where all terms in the equation are functions of position. The tensor D is the deformation potential, which is a material property relating the full strain tensor to the potential V experienced by the charge carrier.

Equation (1) or (2a) is rewritten in a weak form and discretized over a suitable finite element mesh, such as the domain shown in Figure 1. The full finite element formulation is described in detail by Johnson and Freund (2001). The finite element problem amounts to a generalized eigenvalue problem, with n·q solutions, where n is the number of nodes in the mesh, and q is the number of energy subbands in the basis of choice. For the results described in the following sections q is chosen to be one, so the conduction band and valence subbands are considered to be energetically decoupled and are solved independently.

To illustrate the available energy levels, Figure 2 shows schematically a single one-dimensional quantum well with conduction band and valence band components. Within both the conduction band well and the valence band well there are discrete, allowable energy levels with corresponding wave functions increasing in spatial complexity at energies further from the band gap. In the real system of interest, each quantum dot in the array is equivalent to a comparable three-dimensional conduction and valence band quantum well pair. The energy levels shown in Figure 2 are important in the evaluation of the system optical conductivity, which is described in the following subsection.

2.3 Optical conductivity

A simplified view of optical emission and optical absorption is adopted here; either process is considered to be possible for frequencies of light corresponding to peaks in the system optical conductivity. Following Davies (1998), absorption of energy from an incident plane wave of light is described by the real part of the optical conductivity (which can alternatively be expressed as the imaginary part of the dielectric function) and is written for a quantum dot system as:

$$\sigma_1(\omega) = \frac{2\pi}{\Omega\omega}\left(\frac{e}{m_0}\right)^2 \sum_{i,j} |\,\mathbf{e}\cdot\mathbf{p}_{i,j}\,|^2 |< i \mid j >|^2 \delta\left(E_i - E_j - \hbar\omega\right) \tag{4}$$

where ω is the frequency of incident light, Ω is the volume of the system, m_0 is the mass of an electron in free space, e is the fundamental charge, e·p is the inner product of the light polarization vector and the momentum vector of the interacting electron, and i and j are any pair of conduction band and valence band states.

Since the e·p term is fixed for states in particular energy subbands and only the relative magnitude of σ_1 at various frequencies is of interest, the calculation of energy levels and wave functions from the previous step is all that is needed to evaluate equation (4). In the context of Figure 2, given the known electron energy levels and wave functions, vertical transitions mediated by photons of a particular energy can be directly determined.

Thus, for a particular quantum dot morphology such as is shown in Figure 1, energy levels and wave functions are found by solving the Schrödinger equation using the method described in the previous subsection, and optical conductivity is directly evaluated through equation (4). The magnitude of the optical conductivity is then directly comparable to the experimental photoemission and absorption spectra as a function of frequency of light. Details of the experimental measurement under consideration are described in the following subsection.

2.4 Strain due to tip-sample interaction

The experimental setup considered in the model described here is shown in Figure 3. Details of the experiment are described by Robinson et al. (1998, 2001), but are briefly summarized here. A tapered SiO_2 optical fiber is used simultaneously as an optical probe and a nanomechanical indenter. The fiber has an aperture diameter of approximately 250nm, with a flat surface formed as a result of a brittle cleavage fracture. When electron energy level transitions are stimulated by a remote light source, photons are emitted by individual quantum dots according to the frequencies allowed by equation (4). The optical fiber probe collects the emitted photons from approximately 30 quantum dots which lie beneath the aperture. The collected signal is processed to yield an intensity vs. emitted light frequency spectrum.

The probe is used as an indenter by pushing the sample, which rests on a rigid platen, up into contact with the tip. When the sample is pushed further (referred to here as sample displacement), the tip indents the surface and produces an elastic strain field in the sample. The sample displacement is on the order of 10 nanometers, leading to indentation depths on the order of a nanometer, since the overall system compliance is largely due to the elastic behavior of the tip. Forces required to indent further could cause the long probe tip to buckle or could lead to dislocation nucleation in the sample. Dislocations would be expected to damage the electrical and optical properties of the sample by generating charged defects in the otherwise single crystalline material.

Since the SiO_2 fiber is much stiffer than the sample, it can be viewed as a rigid cylindrical flat punch indenter for the purposes of the elasticity problem. The solution for the elastic fields in the substrate material for such a configuration is attributed to Sneddon (1946). The present problem is equivalent to Sneddon's solution of the problem to the extent that the quantum dot sample can be viewed as a homogeneous elastic half-space. This assumption is reasonable since the elastic properties of the $Al_{0.35}Ga_{0.65}As$ and $In_{0.55}Al_{0.45}As$ layers are similar.

In Sneddon's analysis a cylindrical polar coordinate system is adopted, where $\zeta=z/a$ and $\rho=r/a$ are dimensionless parameters defined in terms of distance z below the sample surface, radial coordinate r from the center of the indenter, and the indenter radius a. If the tip is indented a distance ε below the undisturbed surface of the sample, the stress components in the substrate are given by

$$(5a) \qquad \sigma_z = -\frac{4\mu(\lambda+\mu)}{\lambda+2\mu}\frac{\varepsilon}{\pi a}(J_1^0 + \zeta J_2^0)$$

$$(5b) \qquad \tau_{zr} = -\frac{4\mu(\lambda+\mu)}{\lambda+2\mu}\frac{\varepsilon}{\pi a}\zeta J_2^1$$

$$(5c) \qquad \sigma_\theta = -\frac{4\lambda\mu}{\lambda+2\mu}\frac{\varepsilon}{\pi a}J_1^0 - \frac{4\mu^2}{\rho(\lambda+2\mu)}\frac{\varepsilon}{\pi a}(J_1^0 - \frac{\lambda+\mu}{\mu}\zeta J_2^1)$$

where λ and μ are Lamé's elastic constants and J_n^m refers to the integral

$$(6) \qquad J_n^m = \int_0^\infty p^{n-1} \sin(p) \exp(-p\zeta) J_m(p\rho) dp$$

with J_m being the first order Bessel function of the m^{th} kind. Given this full-field stress solution and the elastic constants of the material, it is straightforward to solve for the components of strain at the nodal points in the finite element discretization of the system, part of which is shown in Figure 1. Then, using equation (3), the indentation strain is converted to a scalar potential field.

In this way, an analytical and computational continuum elasticity result is directly coupled to the quantum mechanical formulation through the deformation potential approach. The tip-sample interaction effect can be considered by recalculating the optical spectrum at each sample displacement (indentation depth) of interest. In the following section the results of the simulation are presented and discussed.

3. RESULTS AND DISCUSSION

3.1 The optical spectrum and typical electron states

The principal result of the simulation is the optical conductivity spectrum for the quantum dot array. Figure 4 shows the optical conductivity of the un-indented quantum dot array as a function of frequency. For the purposes of comparison with the experiment, the spectrum is interpreted as a measure of optical absorption and emission. In practice, light of all frequencies with non-zero conductivity may be absorbed, but emitted light frequencies fall in the lower energy range.

The computed spectrum is directly comparable and in reasonable quantitative agreement with the experimental spectrum measured by Robinson *et al.* (1998). The experimental spectrum, which measures only emission, is centered at approximately 1890 meV. The roughly Gaussian distribution of the broad emission/absorption peak is also in agreement with the experimental finding, and is a consequence of the distribution in dots sizes and shapes. Each peak in the overall spectrum corresponds to a transition in a single quantum dot between a computed conduction band state and a computed valence band state.

An example of a representative computed conduction band state is shown in Figure 5a. The key feature of the state is that it is localized to a single quantum dot, and it has approximately spherical symmetry, which is the simplest and lowest energy result. By contrast, a higher energy conduction band state is shown in Figure 5b. This delocalized or extended state has implications for interpreting several experimental observations, including the presence of particular photoemission resonances. This mechanism is described elsewhere. (Johnson *et al.* 2002)

3.2 Indentation strain effect on the optical spectrum

The tip-sample interaction described in the previous section influences both individual quantum dot states such as the ones shown in Figure 5 as well as the overall emission/absorption spectra. The probe, which is used to collect the emitted light that generates the emission spectrum, is also used as a nanomechanical indenter. Through the deformation potential, the indentation strain imposes an effective potential on the quantum dot electron confinement. This phenomenon is illustrated in Figure 6. Here the indentation strain, taken from Sneddon's solution of the Boussinesq problem, is converted to an effective potential and superimposed on the other sources of potential – the energy band structure and the lattice mismatch strain. The strain locally increases the potential, but the effect is nonuniform even over the section of the array contained within the simulation cell.

The experimental photoemission measurement is simulated by computing absorption/emission spectra for the various indentation depths such as are shown in Figure 6. Since each measured spectrum is of the form shown in Figure 4, with hundreds of distinct peaks, it is more illustrative to isolate the emission energies for a few representative quantum dots. It is possible in both the experiment and the simulation to do so. In Figure 7, the computed emission energies of several representative quantum dots are shown in comparison with the measured emission energies for several dots in the experimental study of Robinson *et al.* (1998). It is important to note that these dots in the simulation are not meant to correspond directly to individual dots in the experiment; the dots are merely examples taken from a similar array.

As shown in Figure 7, emission energies for individual dots shift to higher levels as the probe indents the sample. The effect is considered to be a blue shift since indented dots emit at lower wavelengths, although still within the infrared range. The effect is nonlinear and varies between dots, but the simulation shows an approximate shift in wavelength of 0.3nm per nanometer of sample displacement.

While individual dot emission lines are not precisely predicted, the level of agreement is unprecedented in the literature. The dot sizes and shapes are the result of simulation, and the only input

parameters throughout the model are processing parameters and bulk material properties. For comparison, the reasonable but simple argument used by Robinson *et al.* (1998) to explain the indentation energy shift deviated from the observed values by an order of magnitude.

Several features of the indentation energy shift remain to be interpreted. For example, the energy shift varies appreciably from one dot to another, particularly in the experimental measurement, but also in the simulation. This is due in part to the size variation among dots, but is more directly related to the variation in indentation strain as a function of position in the array. Figure 6 shows that the strain-induced potential field varies significantly across the array even for a perfectly normal contact angle. In the experiment it is possible that the nanomechanical probe contacts the surface at an off-normal angle, which would induce a more nonuniform strain. But even with the flat contact assumption, the simulation shows an apparent relationship between dot radial position and energy shift magnitude, as shown in Figure 8. Directly beneath the radial center of the nanomechanical indenter the strain effect on the emission energy is largest.

Finally, another mechanical effect is suggested by the results shown in Figure 7. While the computed emission energies continue to increase as a function of indentation depth, several of the quantum dot emission lines stop at a sample displacement of 10 or 15 nm. In the calculation it is assumed that the indentation strain is elastic, at least within the region of the quantum dots. However, a rigid flat cylindrical indenter induces a singular stress field around its perimeter. This stress field would be expected to lead to dislocation nucleation in the substrate, which would dramatically modify the electronic energy level spectrum at larger indentation depths. Effectively, dislocation activity could "quench" the photoemission of the dots. This phenomenon is currently under investigation.

4. SUMMARY AND CONCLUSIONS

A model for a coupled continuum elastic and quantum mechanical phenomenon is presented here with a specific view toward understanding recent experimental observations. Quantum dots are an important system for possible optoelectronic applications based on the discrete features of the system optical absorption and emission spectra. The experimental result of interest here shows that in measuring these spectra, elastic strain induced through probe-sample interaction can strongly shift the emission energies of the dots.

The model developed here successfully shows the mechanism responsible for the observed optical emission energy shift in the quantum dot array. Results from a previous morphological simulation are used as input to the model in the form of a realistic quantum dot array, with a distribution in size, shape, and spacing of dots. This morphology is generated from only a knowledge of material and processing

parameters. Then, a finite element analysis of the steady-state Schrödinger equation for a single charge carrier in the morphology domain yields the available electron energy states in the system. From these energy states, the optical conductivity is directly evaluated; this can be compared with experimental optical absorption and emission spectra.

This calculation of optical spectra is repeated while considering the effect of strain imposed by the experimental nano-probe that simultaneously collects emitted light and indents the sample. By treating the probe as a rigid cylindrical flat punch in the manner of Sneddon (1946), a full field analytical solution for the strain, which is linearly related to the indentation depth, can be superimposed on the known potential field. Thus, the emission energies as a function of indentation depth are computed; these energies and the approximate optical wavelength shift of 0.3nm per nanometer of sample displacement are in good agreement with experimentally observed values.

The model and simulation are an example of mechanical effects on electronic and optical properties of materials, even at length scales at which quantum mechanical behavior becomes important. The study shows that continuum models for elasticity are valid at the nanometer length scale, and further that there are suitable methods to couple continuum elasticity to simple quantum mechanical models for electronic and optical properties.

ACKNOWLEDGEMENTS

The authors wish to thank Prof. Allan Bower of Brown University for providing the computational mesh from the results of his morphology simulations. The support of NSF Grant No. CMS-0296102 is gratefully acknowledged.

REFERENCES

D. Bimberg, M. Grundmann, and N. N. Ledentsov, *Quantum Dot Heterostructures*, 1st ed., (John Wiley & Sons, Chichester, UK, 1999).

J. H. Davies, *The Physics of Low-Dimensional Semiconductors*, 1st ed., (Cambridge University Press, Cambridge, UK, 1998).

H. T. Johnson and L. B. Freund, "The influence of strain on confined electronic states in semiconductor quantum structures," *Int. J Sol. Struc.* 38, 1049 (2001).

H. T. Johnson, R. Bose, B. B. Goldberg, H. D. Robinson, "Simulation evidence for lateral excitation transfer in a self-assembled quantum dot array," submitted for publication, (2002).

R. Leon, S. Fafard, D. Leonard, J. L. Merz, and P. M. Petroff, "Visible luminescence from semiconductor quantum dots in large ensembles," *Appl. Phys. Lett*. 67, 521 (1995).

H. D. Robinson, M. G. Müller, B. B. Goldberg, and J. L. Merz, "Local optical spectroscopy of self-assembled quantum dots using a near-field optical fiber probe to induce a localized strain field," *Appl. Phys. Lett*. 72, 2081 (1998).

H. D. Robinson, B. B. Goldberg, and J. L. Merz, "Observation of excitation transfer among neighboring quantum dots," *Phys. Rev B.* 64, 075308 (2001).

I. Sneddon, "Boussinesq's problem for a flast-ended cylinder," *Proc. Camb. Phil. Soc*. 42, 29 (1946).

Y. Zhang and A. F. Bower, "Numerical simulations of island formation in a coherent strained epitaxial thin film system," *J. Mech. Phys. Sol*. 47, 2273 (1999).

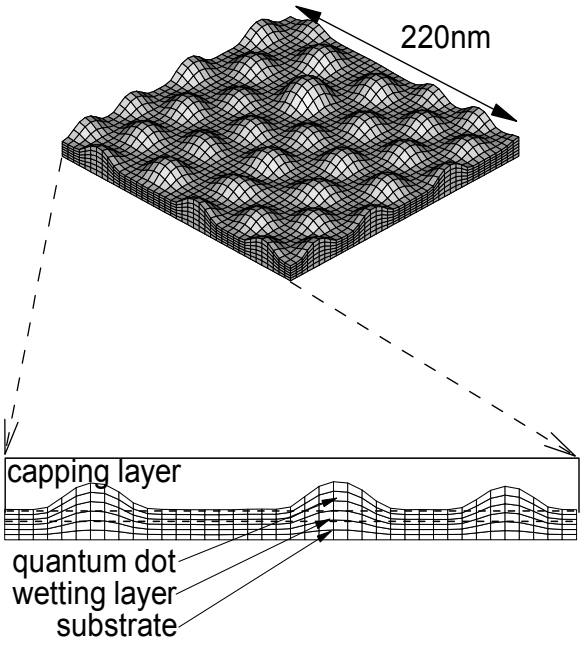

FIG. 1. Computational domain used in the model. The domain includes the substrate, the wetting layer, the quantum dots, and the capping layer. The quantum dots are nonuniform in size, shape, and spacing. For clarity the elements in the capping layer are not shown.

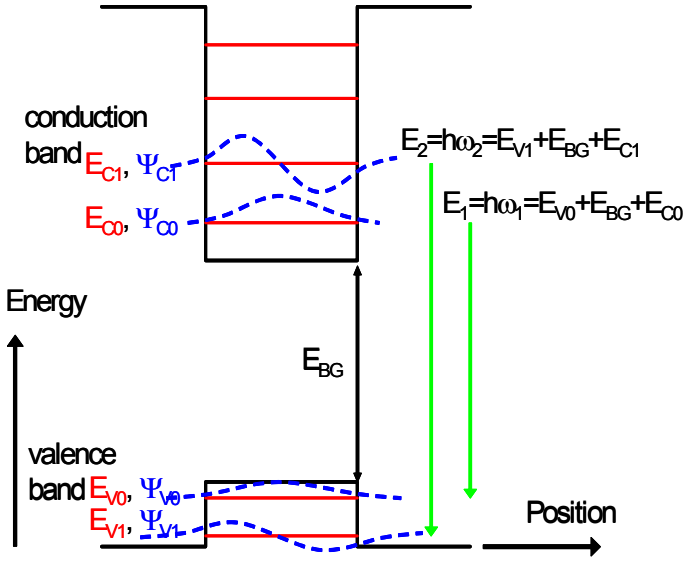

FIG. 2. Schematic of the electron energy levels computed for a single quantum dot. Within the quantum dot region of material, discrete conduction band and valence band energies admit transitions which lead to optical absorption and emission at particular frequencies.

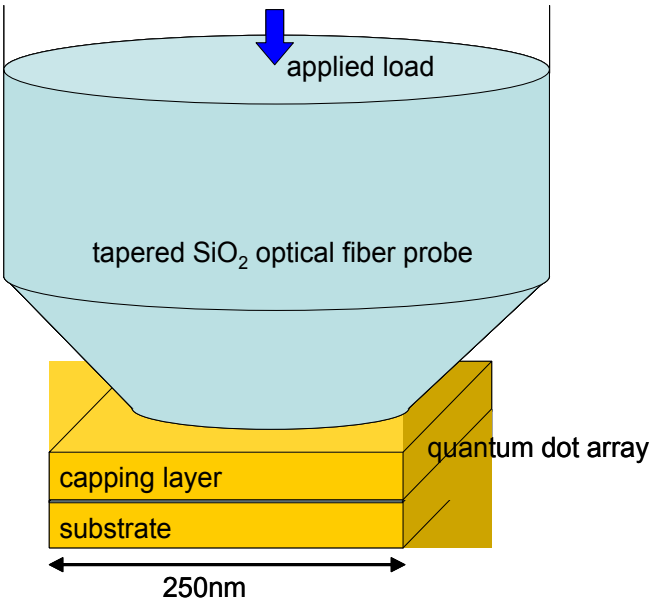

FIG. 3. Schematic of the experimental configuration. The tapered SiO_2 optical fiber is used simultaneously to probe the optical spectra and as a nanomechanical indenter. The embedded quantum dots experience an elastic indentation strain; as a result, the frequency of emitted light shifts.

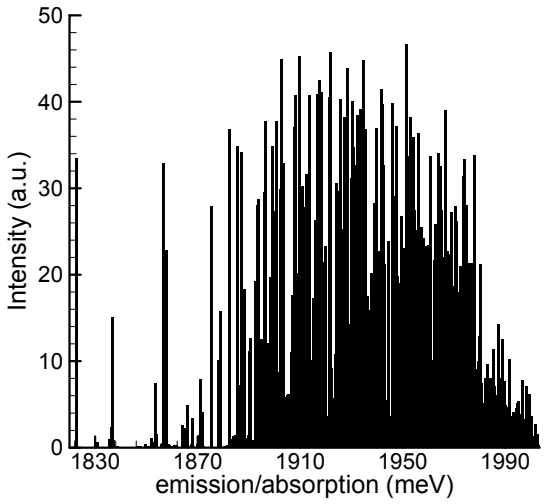

FIG. 4. Computed optical conductivity spectrum for the quantum dot array shown in Figure 1. Conductivity is interpreted as a measure of emission and absorption observed in the experiment. Each peak corresponds to an inter-band transition within an individual quantum dot.

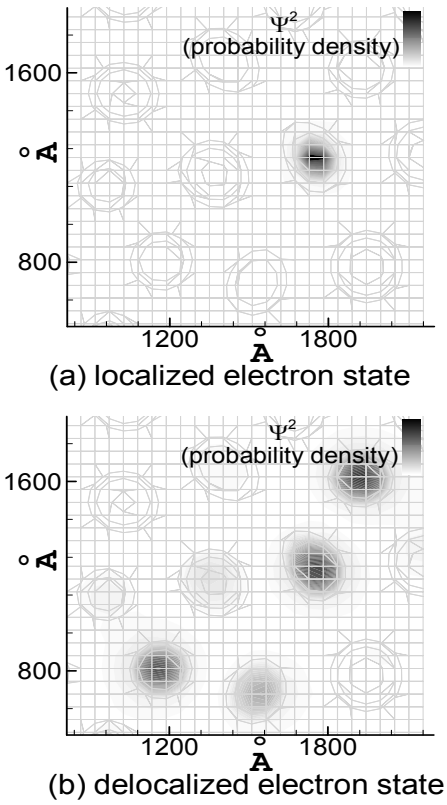

FIG. 5. Cross-sectional views of two representative electron states, plotted as Ψ^2, or probability density. (a) Localized states confined to individual dots are common and are responsible for most optical transitions. (b) At higher energies, some states extend spatially to multiple dots.

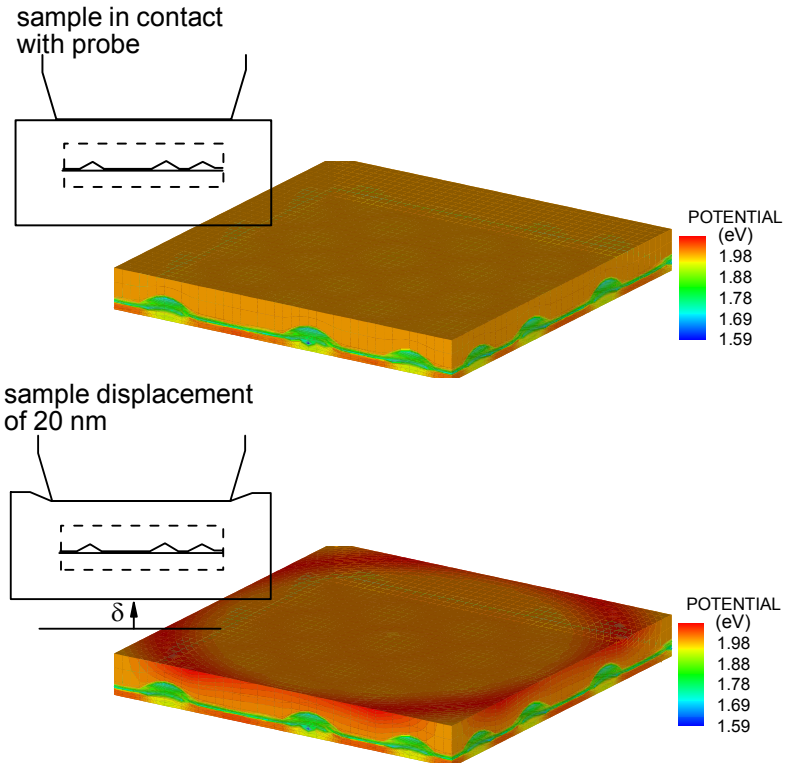

FIG. 6. Effect of indentation on the spatially varying potential field experienced by an electron. The nanomechanical probe is approximately the same size as the simulation domain. The axially symmetric indentation strain field is superimposed as an additional potential.

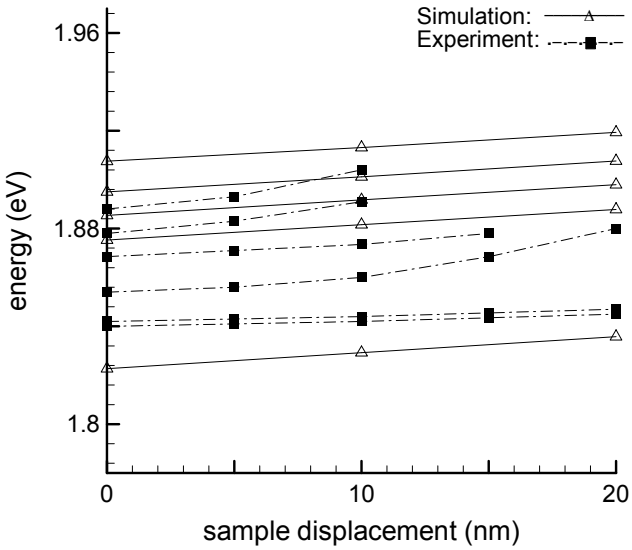

FIG. 7. The effect indentation due to sample displacement on the emission energy of several quantum dots. The simulation data fall in the correct energy range, and the energy shift per unit distance of sample displacement is in close agreement with the experiment. Note that some experimental emission lines are "quenched" by indentation when the sample displacement is more than 10nm.

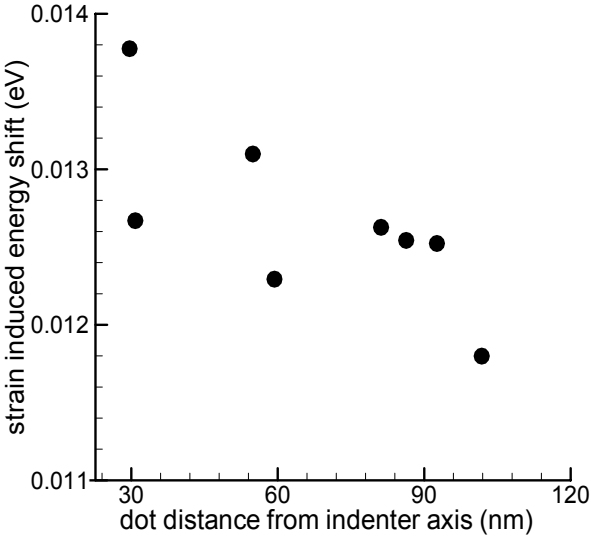

FIG. 8. Relationship between dot position and strain induced energy shift for a representative sample of dots in the array. Near the nanomechanical indenter radial axis the strain induced energy shift is greatest.